PPPL--2675

DE90 010170

Parallel Electric Resistivity in the TFTR Tokamak

M.C. Zarnstorff, K. McGuire, M.G. Bell, B. Grek,

D. Johnson, D. McCune, H. Park,

A. Ramsey, and G. Taylor

Princeton Plasma Physics Laboratory

Princeton University

Princeton, N.J. 08543

I. Introduction

The electrical resistivity of a magnetized plasma parallel to the magnetic field is a basic consequence of the electron parallel force-balance equation. Classical resistivity[1] is predicted for a near-Maxwellian unmagnetized plasma or for a plasma embedded in a uniform magnetic field (in particular $\nabla B = 0$). It is determined by the balance of the electric and friction forces, and includes the consequences of distortion of the electron distribution function away from a shifted Maxwellian. Neoclassical theory[2,3] corrects the classical expression for the effects of a poloidally nonuniform magnetic field strength in an axisymmetric toroidal plasma, in particular the parallel viscous damping due to magnetic trapping or magnetic pumping (for collisionless or collisional electrons, respectively). Thus, experimental measurements of the resistivity are of fundamental importance in understanding parallel electron transport. In some theories, parallel electron transport is closely related to cross-field transport; thus, an understanding of the parallel resistivity can give insight into the mechanisms of anomalous perpendicular transport. In addition, the resistivity is of practical importance in understanding and designing laboratory plasma arcs and pinches, such as tokamaks.

Previous measurements of the plasma resistivity in tokamaks, averaged over the plasma cross section, have been in agreement with the classical value

in PLT,[4] TEXT,[5] ASDEX,[6] and JT-60,[7] have been between the classical and neoclassical values in JET,[8] and have been in agreement with neoclassical theory in a recent reanalysis of JT-60 data.[9] In addition, the resistivity was found to be anomalous when the current was being ramped up or down slowly on JET.[8,10] Local measurements of the resistivity were found to be in agreement with neoclassical theory for toroidal multipoles[11] for the plateau and collisional regimes (but were anomalously large for the collisionless regime), and were between the classical and neoclassical predictions (but did not resolve between them) in the TEXTOR[12] and JET[8] tokamaks (see Ref. 10 for differing conclusions). In other experiments, the resistivity was assumed[13] to be either classical or neoclassical as a way of inferring the plasma impurity content. Previous experiments with high β_P auxiliary heated plasmas on TFTR[14] and JET[15] were found to agree with the predictions of the neoclassical bootstrap current in combination with neoclassical resistivity.

In this paper we compare the resistivity of TFTR ohmic plasmas with theoretical predictions over a wide range of plasma parameters. Section II describes general experimental and plasma conditions, section III discusses the analysis method, section IV presents the experimental results, and section V discusses and summarizes the work.

II. Experimental Conditions

The TFTR experiment has been described previously.[16] The tokamak plasmas studied here were heated ohmically and fueled by gas puffing at the plasma edge. The evolution of global parameters for a typical plasma are shown in Fig. 1.

The TFTR magnetic diagnostics are described in Ref. 17. The plasma current I_P is measured by a poloidal Rogowski loop. The plasma position, shape, and $\Lambda \equiv \beta_P + l_i/2$, are obtained by fitting measured moments of the poloidal magnetic field distribution (by a poloidal array of loops) and the poloidal flux distribution (by six saddle-coils) outside the thin vacuum vessel (vessel field-penetration time $\sim$ 10 msec) using a filament code.[18] Here $\beta_P \equiv 2\mu_0 \bar{p}/B_P^2(a)$ is the poloidal beta, $l_i \equiv \bar{B}_P^2/B_P^2(a)$ is the dimensionless internal inductance, p is the plasma pressure, B_P is the poloidal magnetic field strength, and the overbar indicates volume average. The toroidal voltage at the plasma surface is obtained by averaging the voltages measured on six toroidal loops (distributed poloidally) corrected for the calculated time-derivative of the poloidal flux between each loop and the plasma. The poloidal voltage at the plasma surface is obtained using a poloidal loop (part of the diamagnetic system) corrected for the calculated time-derivative of the toroidal flux between the loop and the plasma. The time-evolution of the

plasma current I_p, plasma horizontal and radial position, and line-average electron density $\bar{n}_e$ (as measured by a horizontal 4 mm interferometer) are controlled by preprogrammed feedback loops.[19]

The electron density n_e and temperature T_e profiles are measured at a single time in each discharge by Thomson scattering,[20] see Fig. 2. The time evolution of the n_e profile is obtained by Abel inversion[21] of the measurements of a ten-channel array of far-infrared interferometers.[22] The time evolution of the T_e profile is measured by electron cyclotron emission (ECE) radiometry[23] calibrated by the Thomson scattering measurement. The time evolution of the n_e and T_e profiles for the plasma of Fig. 1 are shown in Fig. 3. The central $Z_{eff} \equiv \sum n_i Z_i^2 / n_e$, where the sum is over the ion species, is determined from tangential and radial measurements of the visible bremsstrahlung emission,[24] as shown in Fig. 4. Z_{eff} is measured (using an array of visible bremsstrahlung detectors) to be spatially uniform in the helium plasmas studied and in previous deuterium plasmas. It is assumed to be uniform for the deuterium plasmas studied here.

III. Analysis

Two slightly different methods have been used in this study: full time-dependent analysis of an entire discharge using TRANSP[25] and near-equilibrium

analysis at a single time using SNAP.[26] In both cases, the measured plasma kinetic parameters (T_e, n_e) are mapped and symmetrized onto an magnetohydrodynamic equilibrium set of flux surfaces calculated self-consistently using the kinetic pressure profile and the magnetically measured shape and location of the outermost flux surface. The Thomson scattering measurements of the T_e and n_e profiles are each found to be symmetric within $\pm 10\%$ for $r < 0.7\,a$ in the plasmas studied.

TRANSP numerically evolves the poloidal field diffusion equation[2]

$$\frac{\partial}{\partial t}\frac{\partial \psi}{\partial \rho} = \frac{\partial}{\partial \rho}\left[\frac{2\pi\langle \boldsymbol{E}\cdot\boldsymbol{B}\rangle}{F\langle R^{-2}\rangle}\right] \tag{1}$$

on a toroidal flux surface grid, where ψ is the poloidal flux contained within a given flux surface, R is the local major radius, $F = RB_T$, $\boldsymbol{B_T}$ and $\boldsymbol{B}$ are the toroidal and total magnetic field, $\boldsymbol{E}$ is the electric field, ρ is a radial flux surface coordinate, the standard flux surface average is $\langle A\rangle \equiv \partial\rho/\partial V' \oint A\,dS/|\nabla\rho|$, V' is the volume enclosed in the flux surface, and dS is an area element on the flux surface. The measured total plasma current provides the external boundary condition for the solution, and the flux surface averages are evaluated using a moments-solution[27] to the Grad-Shafranov equation using the measured plasma shape and kinetic pressure profile, and the calculated current profile. The parallel electric field on each flux surface is related to the parallel current density J by the flux-surface-averaged

electron parallel force-balance equation, or Ohm's law[3]

$$\langle \boldsymbol{E} \cdot \boldsymbol{B} \rangle = \eta_{\parallel} \langle (\boldsymbol{J} - \boldsymbol{J}_{\mathrm{DR}}) \cdot \boldsymbol{B} \rangle, \tag{2}$$

where $\boldsymbol{J}_{\mathrm{DR}}$ is any current not driven by the electric field and $\eta_{\parallel}$ is the parallel resistivity. The plasma resistivity on each flux surface is calculated from the measured plasma parameters using a theoretically predicted resistivity. The predicted resistivity for a flow-shifted Maxwellian electron distribution function is

$$\eta_{\parallel \mathrm{mx}} = \frac{m_e Z_{eff} \nu_{ee}}{n_e e^2}, \tag{3}$$

where m_e is the electron mass, e is the electron charge, and ν_{ee} is the electron-electron collision frequency.[28] Classical resistivity is accurately given by[29]

$$\eta_{\parallel \mathrm{cl}} = \eta_{\parallel \mathrm{mx}} \left[\frac{1 + 1.198\, Z_{eff} + 0.222\, Z_{eff}^2}{1 + 2.966\, Z_{eff} + 0.753\, Z_{eff}^2} \right], \tag{4}$$

and neoclassical resistivity by[30]

$$\eta_{\parallel \mathrm{nc}} = \eta_{\parallel \mathrm{cl}} \left(1 - \frac{f_t}{1 - \xi \nu_{*e}} \right)^{-1} \left(1 - \frac{c_R f_t}{1 - \xi \nu_{*e}} \right)^{-1}, \tag{5}$$

where f_t is the trapped particle fraction, $c_R = 0.56\, Z_{eff}{}^{-1} (3.0 - Z_{eff})/(3.0 + Z_{eff})$, $\xi = 0.58 + 0.20 Z_{eff}$, $\nu_{*e} \equiv \nu_e/(\epsilon^{3/2} \omega_b)$. ν_e is the electron collision frequency, $\epsilon \equiv r/R$, r is the local minor radius, and ω_b is the electron bounce frequency. The neoclassical resistivity is larger than the classical value due to damping of poloidal electron motion by neoclassical parallel viscosity. Relativistic corrections to the resistivity[31] are negligible, for the plasmas studied,

as $T_e \ll 511$ keV. The only non-Ohmic current $\boldsymbol{J}_{DR}$ predicted for the plasmas studied here is the neoclassical bootstrap current, which arises from the interaction of the Pfirsch-Schlüter current with the neoclassical parallel viscosity. This is calculated using expressions[3,29] including the effects of impurities and finite aspect ratio, and is predicted to be small (but systematically significant) due to the low β_P achieved Ohmically (see Table 1). An optional Kadomtsev sawtooth reconnection model[32] can be applied in TRANSP to redistribute the current profile each time a sawtooth is observed experimentally. In other experiments[33,34] the observed change in the current profile due to sawteeth is less than predicted by the Kadomtsev model; thus, the effects of sawteeth on the current profile evolution should be bounded between no sawtooth-redistribution and the Kadomtsev model.

The results of these calculations are various predictions (for a given theoretical resistivity and sawtooth model) that can be compared with experimental measurements, such as the q profile and the parallel voltage per toroidal transit at the surface of the plasma

$$\begin{aligned} V_{sur} &\equiv \left. \frac{2\pi \langle \boldsymbol{E} \cdot \boldsymbol{B} \rangle}{F \langle R^{-2} \rangle} \right|_a \\ &= \frac{\partial \psi(a)}{\partial t} - \frac{1}{q(a)} \frac{\partial \phi(a)}{\partial t}, \end{aligned} \tag{6}$$

where ϕ is the toroidal flux contained within the flux surface and $q \equiv \partial\phi/\partial\psi$ is the safety factor.

The SNAP analysis is similar to the TRANSP analysis, except that it solves for the steady-state current profile and assumes circular cross-section flux surfaces. In many TFTR plasmas, the current profile does not reach steady state during the finite pulse length available (< 8 sec). In order to analyze these plasmas with SNAP the effective surface voltage $V'_{sur} = V_{sur} - \frac{1}{2}\mu_0 R I_p \partial l_i/\partial t$ is used, approximately correcting for the extra voltage due to the equilibrating inductance. This expression for V'_{sur} above has taken advantage of the restriction of the SNAP analysis to times when $\partial I_P/\partial t = \partial R(a)/\partial t = 0$. For all of the SNAP results discussed here the inductance is nearly equilibrated, with less than a 10% difference between V_{sur} and V'_{sur}.

IV. Experimental Results

The resistivity has been analyzed for a wide variety of ohmic plasmas from the 1986, 1987, and 1988 TFTR runs, whose parameters are summarized in Table 1 and Fig. 5. These plasmas were selected by having an adequate set of diagnostic measurements, by not showing significant distortion of their ECE spectrum (which would indicate the presence of high-energy nonthermal electrons), and by not being detached[35] or having a MARFE.[36] Figure 6 compares the measured evolution of V_{sur} for the plasma of Fig. 1 with the TRANSP predictions using classical and neoclassical resistivity. The

predictions of the two theories are well separated throughout the discharge, and the neoclassical prediction is in good agreement with the measurement throughout (including the slow I_P ramp-up and -down phases). Due to the low β_P achieved ohmically, the calculated total bootstrap current is small ($\sim$ 100 kA), decreasing the neoclassical V_{sur} by 5.5% during the I_P-constant period. The possible effect of Kadomtsev sawtooth reconnection is very small, and is calculated to increase the neoclassical V_{sur} by less than 1% relative to the curve in Fig. 6. The results of similar analysis using TRANSP and SNAP are summarized in Fig. 7 for the plasmas of Fig. 5. The uncertainties shown in the figures represent the standard deviation of the distribution of results obtained by varying all of the experimental measurements within their range of uncertainty (both systematic and statistical), as estimated by a Monte-Carlo ensemble. On the average, 49% of the calculated uncertainty in V_{sur} is due to uncertainty in T_e, 33% is from uncertainty in the visible bremsstrahlung signal, and 18% is from uncertainty in the n_e profile shape. In general, the measurements indicate that the average resistivity is equal to the neoclassical prediction within the experimental uncertainty. It should be noted that, while the average experimental resistivity is roughly twice the classical prediction, there is not a constant ratio between them. As shown in Fig. 8, this ratio varies (modestly) with electron collisionality ν_{*e} as ex-

pected from neoclassical theory. In particular, see Fig. 8(c), the observed resistivity is in disagreement with the value expected for purely Maxwellian electrons. Taken as an ensemble, the data of Fig. 8 indicate that the ratio of the neoclassically predicted V_{sur} to the measured V_{sur} is 1.014 ± 0.057.

While a direct measurement of the plasma current or q profile was not available for these experiments, experimental information about the current profile shape can be obtained from the location of the $q = 1$ surface. The $q = 1$ surface can be unambiguously located by observation of the initial position of the $m/n = 1/1$ sawtooth precursor, as measured by a high speed soft x-ray camera.[37] In addition, the sawtooth inversion radius typically agrees well with the $m/n = 1/1$ position, and gives a more generally available indication of the $q = 1$ minor radius. Figure 9 compares the calculated radius of the $q = 1$ surface (with and without the Kadomtsev sawtooth model) with the observed sawtooth inversion radius (also measured by the soft x-ray camera) and the observed $m/n = 1/1$ location for the plasma of Fig. 1. The neoclassical-resistivity calculation accurately predicts the evolution of the $q = 1$ radius, including the coincidence of the initial appearance of a $q = 1$ surface and the first observed sawtooth. In contrast, the classical-resistivity prediction shows no $q = 1$ surface during the entire discharge, in clear conflict with the observed sawteeth and the measured $q = 1$ location. With classical

resistivity, the minimum value of q predicted for this discharge is 1.2, occurring at the end of the analysis ($\sim$ 5 sec) when I_P has dropped to 0.7 MA. For all the plasmas studied, the predicted and measured radius of the $q = 1$ surface were found to agree with neoclassical resistivity, and no $q = 1$ surface was predicted with classical resistivity. The time evolution of Λ also gives an integral measure of the current profile shape. While the measured evolution and value of Λ is generally in better agreement with the neoclassical prediction than the classical prediction, the difference between the two predictions is usually not large enough to be experimentally significant.

V. Discussion

The above observations indicate that the parallel plasma resistivity is in good agreement with the predictions of neoclassical parallel-transport theory over a wide range of plasma parameters from the banana regime into the plateau regime. This agreement is found when the plasma current is static or is being ramped up or down at a moderate rate ($\partial I_P/\partial t \leq 1$ MA/sec). No attempt has been made to analyze the very rapid initial current ramp ($\partial I_P/\partial t \geq 5$ MA/sec during the first 0.2 sec) on TFTR.

While the observations indicate that the parallel electron transport is as expected from neoclassical theory, the observed perpendicular transport

is typically much larger (by a factor $\gtrsim 100$) than neoclassical predictions. This combination is expected, for example, if the perpendicular transport is dominantly caused by electrostatic turbulence.[38] It is easily seen that if the perpendicular diffusion coefficient for electron parallel momentum is comparable to the observed perpendicular electron thermal diffusion coefficient ($\chi_e \sim 1$ m^2/sec), the effect on the apparent resistivity is negligible. Alternatively, it has been proposed[39–41] that an adequate self-consistent explanation of the anomalous perpendicular transport could be obtained via an anomalously large ν_{ee}, possibly due to the interaction between the electrons and turbulent structures. Such an increase in ν_{ee} increases the parallel viscosity (in the collisionless regime), and thus increases the resistivity, bootstrap current, and Ware pinch over the neoclassical values. The increased resistivity and bootstrap current largely cancel, resulting in the overall appearance of classical resistivity,[40] for an ohmic plasma that remains in the collisionless regime. The general case is more complicated,[41] but consistently leads to the appearance of anomalous (non-neoclassical) resistivity. This is in conflict with the above observations, indicating that it is very unlikely that an anomalous ν_{ee} is the cause of anomalous perpendicular transport.

Finally, the persistent and long-standing observations of classical resistivity in small tokamaks[4–6] stand in sharp contrast to the observations presented

here. Due to the fundamental connection between the parallel resistivity and parallel (and some perpendicular) transport processes, this may imply that the electron transport mechanisms are fundamentally different in large and small tokamak experiments.

In conclusion, the ohmic resistivity and general current profile shape in TFTR is seen to be in good agreement with neoclassical predictions for the available range of plasma parameters for both near-equilibrium and dynamic (current changing) situations. The observed resistivity is in disagreement with predictions neglecting toroidal (trapped particle) effects or involving significantly anomalous resistivity in conjunction with anomalous transport.

Acknowledgments

We are grateful for the support of the TFTR group and for discussions with J.D. Callen, R.J. Goldston, R.J. Hawryluk, D.M. Meade, S. Scott, and P. Terry.

This work was supported by US Department of Energy contract DE-AC02-76-CHO-3073.

References

[1]L. Spitzer, Jr. and R. Härm, Phys. Rev. **89**, 977 (1953).

[2]F. L. Hinton and R. D. Hazeltine, Rev. Mod. Phys. **42**, 239 (1976).

[3]S. P. Hirshman and D. J. Sigmar, Nucl. Fusion **21**, 1079 (1981).

[4]E. Meservey, M. Bitter, C. Daughney, D. Eames, P. Efthimion, E. Hinnov, R. Hulse, D. Post, K. Sato, S. Suckewer, and S. von Goeler, Nucl. Fusion **24**, 3 (1984).

[5]J. L. Porter, P. E. Phillips, S. C. McCool, S. B. Kim, D. W. Ross, W. H. Miner, and J. C. Wiley, Nucl. Fusion **27**, 205 (1987).

[6]H. Röhr, K. H. Steuer, and the ASDEX Team, Rev. Sci. Instrum. **59**, 1875 (1988).

[7]T. Hirayama, K. Shimizu, H. Shirai, M. Kikuchi, N. Hosogane, H. Yoshida, and JT-60 Team, in *Proceedings of the 15th European Conference on Controlled Fusion and Plasma Heating*, EPS, Geneva, 1988, volume 3, p. 1065.

[8]D. V. Bartlett, R. J. Bickerton, M. Brusati, D. J. Campbell, J. P. Christiansen, J. G. Cordey, S. Corti, A. E. Costley, A. Edwards, J. Fessey, M. Gadeberg, A. Gibson, R. D. Gill, N. Gottardi, A. Gondhalekar, C. W.

Gowers, F. Hendriks, O. N. Jarvis, E. Källne, J. Källne, S. Kissel, L. C. J. M. De Kock, H. Krause, E. Lazzaro, P. J. Lomas, F. K. Mast, P. D. Morgan, P. Nielsen, R. Prentice, R. T. Ross, J. O'Rourke, G. Sadler, F. C. Schüller, M. F. Stamp, P. E. Stott, D. R. Summers, A. Tanga, A. Taroni, P. R. Thomas, F. Tibone, G. Tonetti, B. J. D. Tubbing, and M. L. Watkins, Nucl. Fusion **28**, 73 (1988).

[9]M. Kikuchi, M. Azumi, S. Tsuji, K. Tani, and H. Kubo, Nucl. Fusion **30**, 343 (1990).

[10]D. J. Campbell, E. Lazzaro, M. F. F. Nave, J. P. Christiansen, J. G. Cordey, F. C. Schüller, and P. R. Thomas, Nucl. Fusion **28**, 981 (1988).

[11]J. F. Etzweiler and D. A. Brouchous, Phys. Fluids **23**, 2547 (1980).

[12]H. Soltwisch, E. Graffmann, J. Schlüter, and G. Waidmann, in *Proceedings of the International Conference on Plasma Physics, Invited Papers (Lausanne)*, edited by M. Q. Tran and R. J. Verbeek, CEC, Brussels, 1984, volume 1, p. 499.

[13]R. M. Wieland, H. C. Howe, E. A. Lazarus, M. Murakami, and C. E. Thomas, Nucl. Fusion **23**, 447 (1983).

[14]M. C. Zarnstorff, M. G. Bell, M. Bitter, R. J. Goldston, B. Grek, R. J.

Hawryluk, K. Hill, D. Johnson, D. McCune, H. Park, A. Ramsey, G. Taylor, and R. Wieland, Phys. Rev. Lett. **60**, 1306 (1988).

[15]C. D. Challis, J. G. Cordey, H. Hamnén, P. M. Stubberfield, J. P. Christiansen, E. Lazzaro, D. G. Muir, D. Stork, and E. Thompson, Nucl. Fusion **29**, 563 (1989).

[16]R. J. Hawryluk, V. Arunasalam, M. G. Bell, M. Bitter, W. R. Blanchard, N. L. Bretz, R. Budny, C. E. Bush, J. D. Callen, S. A. Cohen, S. K. Combs, S. L. Davis, D. L. Dimock, H. F. Dylla, P. C. Efthimion, L. C. Emerson, A. C. England, H. P. Eubank, R. J. Fonck, E. Fredrickson, H. P. Furth, G. Gammel, R. J. Goldston, B. Grek, L. R. Grisham, G. Hammett, W. W. Heidbrink, H. W. Hendel, K. W. Hill, E. Hinnov, S. Hiroe, H. Hsuan, R. A. Hulse, K. P. Jaehnig, D. Jassby, F. C. Jobes, D. W. Johnson, L. C. Johnson, R. Kaita, R. Kamperschroer, S. M. Kaye, S. J. Kilpatrick, R. J. Knize, H. Kugel, P. H. LaMarche, B. LeBlanc, R. Little, C. H. Ma, D. M. Manos, D. K. Mansfield, R. T. McCann, M. P. McCarthy, D. C. McCune, K. McGuire, D. H. McNeill, D. M. Meade, S. S. Medley, D. R. Mikkelsen, S. L. Milora, W. Morris, D. Mueller, V. Mukhovatov, E. B. Nieschmidt, J. O'Rourke, D. K. Owens, H. Park, N. Pomphrey, B. Prichard, A. T. Ramsey, M. H. Redi, A. L. Roquemore, P. H. Rutherford, N. R. Sauthoff, G. Schilling, J. Schivell, G. L. Schmidt,

S. D. Scott, S. Sesnic, J. C. Sinnis, F. J. Stauffer, B. C. Stratton, G. D. Tait, G. Taylor, J. R. Timberlake, H. H. Towner, M. Ulrickson, V. Vershkov, S. von Goeler, F. Wagner, R. Wieland, J. B. Wilgen, M. Williams, K. L. Wong, S. Yoshikawa, R. Yoshino, K. M. Young, M. C. Zarnstorff, V. S. Zaveryaev, and S. J. Zweben, in *Plasma Physics and Controlled Nuclear Fusion Research*, IAEA, Vienna, 1987, volume 1, p. 51.

[17]J. Coonrod, M. G. Bell, R. J. Hawryluk, D. Mueller, and G. D. Tait, Rev. Sci. Instrum. **56**, 941 (1985).

[18]D. W. Swain and G. H. Neilson, Nucl. Fusion **22**, 1015 (1982).

[19]R. D. Woolley, M. G. Bell, J. Coonrod, P. Efthimion, R. J. Hawryluk, W. Hojsak, R. J. Marsala, D. Mueller, W. Rauch, G. D. Tait, G. Taylor, and M. Thompson, Fusion Tech. **8**, 1807 (1985).

[20]D. Johnson, N. Bretz, D. Dimock, B. Grek, D. Long, R. Palladino, and E. Tolnas, Rev. Sci. Instrum. **57**, 1856 (1986).

[21]H. Park, Plasma Phys. Controlled Fusion **31**, 2035 (1989).

[22]D. K. Mansfield, H. K. Park, L. C. Johnson, H. M. Anderson, R. Chouinard, V. S. Foote, C. H. Ma, and B. J. Clifton, Appl. Opt. **26**, 4469 (1987).

[23]G. Taylor, P. Efthimion, M. McCarthy, V. Arunasalam, R. Bitzer, J. Bryer,

R. Cutler, E. Fredd, M. A. Goldman, and D. Kaufman, Rev. Sci. Instrum. **55**, 1739 (1984).

[24]A. T. Ramsey and S. L. Turner, Rev. Sci. Instrum. **58**, 1211 (1987).

[25]R. J. Hawryluk, in *Physics of Plasmas Close to Thermonuclear Conditions*, edited by B. Coppi et al., CEC, Brussels, 1980, volume 1, p. 19.

[26]H. Towner and R. J. Goldston, Bull. Am. Phys. Soc. **29**, 1305 (1984).

[27]L. L. Lao, R. M. Wieland, W. A. Houlberg, and S. P. Hirshman, Computer Phys. Comm. **27**, 129 (1982).

[28]S. I. Braginskii, in *Reviews of Plasma Physics*, Consultants Bureau, New York, 1965, volume 1, p. 205.

[29]S. P. Hirshman, Phys. Fluids **21**, 1295 (1978).

[30]S. P. Hirshman, R. J. Hawryluk, and B. Birge, Nucl. Fusion **17**, 611 (1977).

[31]B. J. Braams and C. F. F. Karney, Phys. Fluids B **1**, 1355 (1989).

[32]B. B. Kadomtsev, Sov. J. Plasma Phys. **1**, 389 (1975).

[33]T. H. Osborne, R. N. Dexter, and S. C. Prager, Phys. Rev. Lett. **49**, 734 (1982).

[34]H. Soltwisch, Rev. Sci. Instrum. **59**, 1599 (1988).

[35]J. D. Strachan, F. P. Boody, C. E. Bush, S. A. Cohen, B. Grek, L. Grisham, F. C. Jobes, D. W. Johnson, D. K. Mansfield, S. S. Medley, W. Morris, H. K. Park, J. F. Schivell, G. Taylor, K. L. Wong, S. Yoshikawa, M. C. Zarnstorff, and S. J. Zweben, J. Nucl. Mater. **145-147**, 186 (1987).

[36]B. Lipschultz, B. LaBombard, E. S. Marmar, M. M. Pickrell, J. L. Terry, R. Watterson, and S. M. Wolfe, Nucl. Fusion **24**, 977 (1984).

[37]K. McGuire, R. J. Colchin, E. Fredrickson, K. Hill, L. C. Johnson, W. Morris, V. Pare, N. Sauthoff, and S. von Goeler, Rev. Sci. Instrum. **57**, 2136 (1986).

[38]K. C. Shaing, Phys. Fluids **31**, 2249 (1988).

[39]G. V. Pereverzev and P. N. Yushmanov, Sov. J. Plasma Phys. **6**, 543 (1980).

[40]J. W. Connor and J. B. Taylor, Comments Plasma Phys. Controlled Fusion **11**, 37 (1987).

[41]L. Kovrizhnykh, Sov. J. Plasma Phys. **14**, 834 (1988).

Tables

TABLE I. The range of discharge parameters for the plasmas studied.

Ion Species	D, He, C
I_P	0.7 - 2.2 MA
B_T	3.9 - 5.1 T
R	2.3 - 2.5 m
R/a	3.0 - 3.6
$\bar{n}_e$	0.5 - 9.0 $\times 10^{19}$ m^{-3}
$T_e(0)$	1.8 - 5.4 keV
Z_{eff}	1.4 - 6.4
β_P	0.06 - 0.36

Figures

FIG. 1. Time evolution of I_P, R, Λ, V_{sur}, and $\bar{n}_e$ the line-average electron density for a typical helium TFTR Ohmic plasma.

FIG. 2. Radial profiles of (a) T_e and (b) n_e, measured in the horizontal midplane by Thomson scattering for the plasma of Fig. 1 at $t = 3.9$ sec. The error bars represent the standard deviation in the value from the fit to the scattered spectrum. The systematic uncertainty of T_e is calculated to have a standard deviation of 5% of the measured values.

FIG. 3. Contour plots of the time evolution of the (a) T_e and (b) n_e profiles for the plasma of Fig. 1, as measured by ECE spectroscopy (calibrated to Thomson scattering) and the interferometer array, respectively. Contour intervals (and lowest contour values) are 200 eV and 5×10^{18} m^{-3}, respectively.

FIG. 4. The time evolution of Z_{eff} for the plasma of Fig. 1, calculated from a visible bremsstrahlung measurement along a tangentially viewing chord.

FIG. 5. Range of plasma parameters studied, where $q(a)$ is the edge safety factor and $\nu_{*e}(a/2)$ is the electron collisionality parameter at $r = a/2$. Solid circles (•) indicate helium plasmas (at the end of the constant current period) analyzed using TRANSP, open circles (○) indicate helium

plasmas analyzed using SNAP, and (×) indicate deuterium plasmas analyzed using SNAP.

FIG. 6. Time evolution of V_{sur} for the plasma of Fig. 1: (a) measured, (b) predicted using neoclassical resistivity, and (c) predicted using classical resistivity.

FIG. 7. Predicted values of V_{sur} (for (a) neoclassical and (b) classical resistivity) vs. measured values. Solid circles (•) indicate helium plasmas (at the end of the constant current period) analyzed using TRANSP, open circles (○) indicate helium plasmas analyzed using SNAP, and (×) indicate deuterium plasmas analyzed using SNAP.

FIG. 8. Ratio of predicted to measured values of V_{sur} vs. ν_{*e} at $r = a/2$, for (a) neoclassical, (b) classical resistivity, and (c) the flow-shifted Maxwellian resistivity. Solid circles (•) indicate helium plasmas (at the end of the constant current period) analyzed using TRANSP, open circles (○) indicate helium plasmas analyzed using SNAP, and (×) indicate deuterium plasmas analyzed using SNAP.

FIG. 9. Time evolution of the radius of the $q = 1$ surface: (a) $m/n = 1$ precursor radius, (b) sawtooth inversion radius, (c) predicted using neoclassical resistivity without redistribution of the current profile by saw-

teeth, and (d) predicted using neoclassical resistivity and the Kadomtsev sawtooth model. The prediction using classical resistivity does not have a $q = 1$ surface in the plasma at any time.

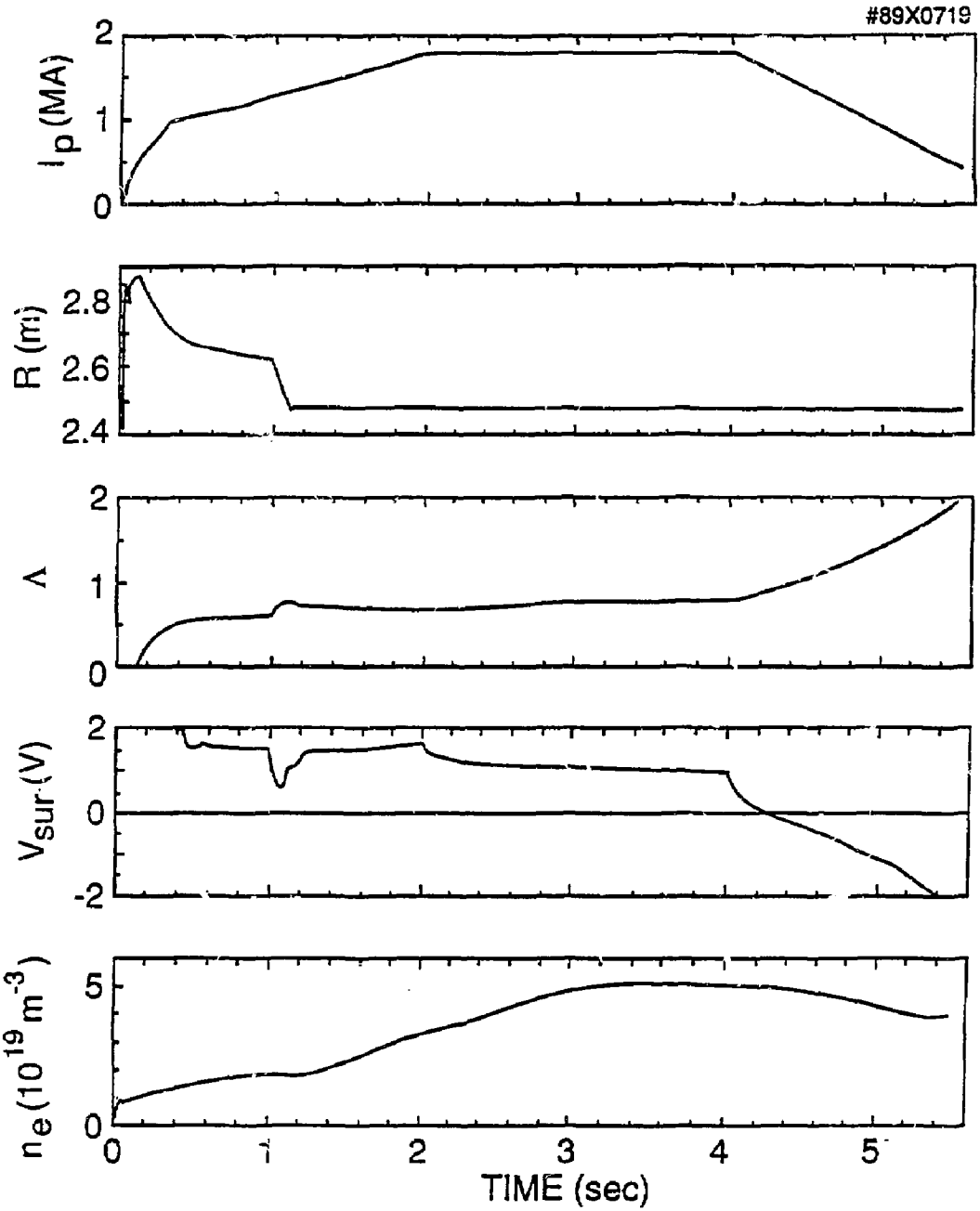
#89X0719
I_p (MA)
2
1
0
R (m)
2.8
2.6
2.4
Λ
2
1
0
V_{sur} (V)
2
0
-2
n_e (10^{19} m^{-3})
5
0
0
1
2
3
4
5
TIME (sec)

FIG. 1

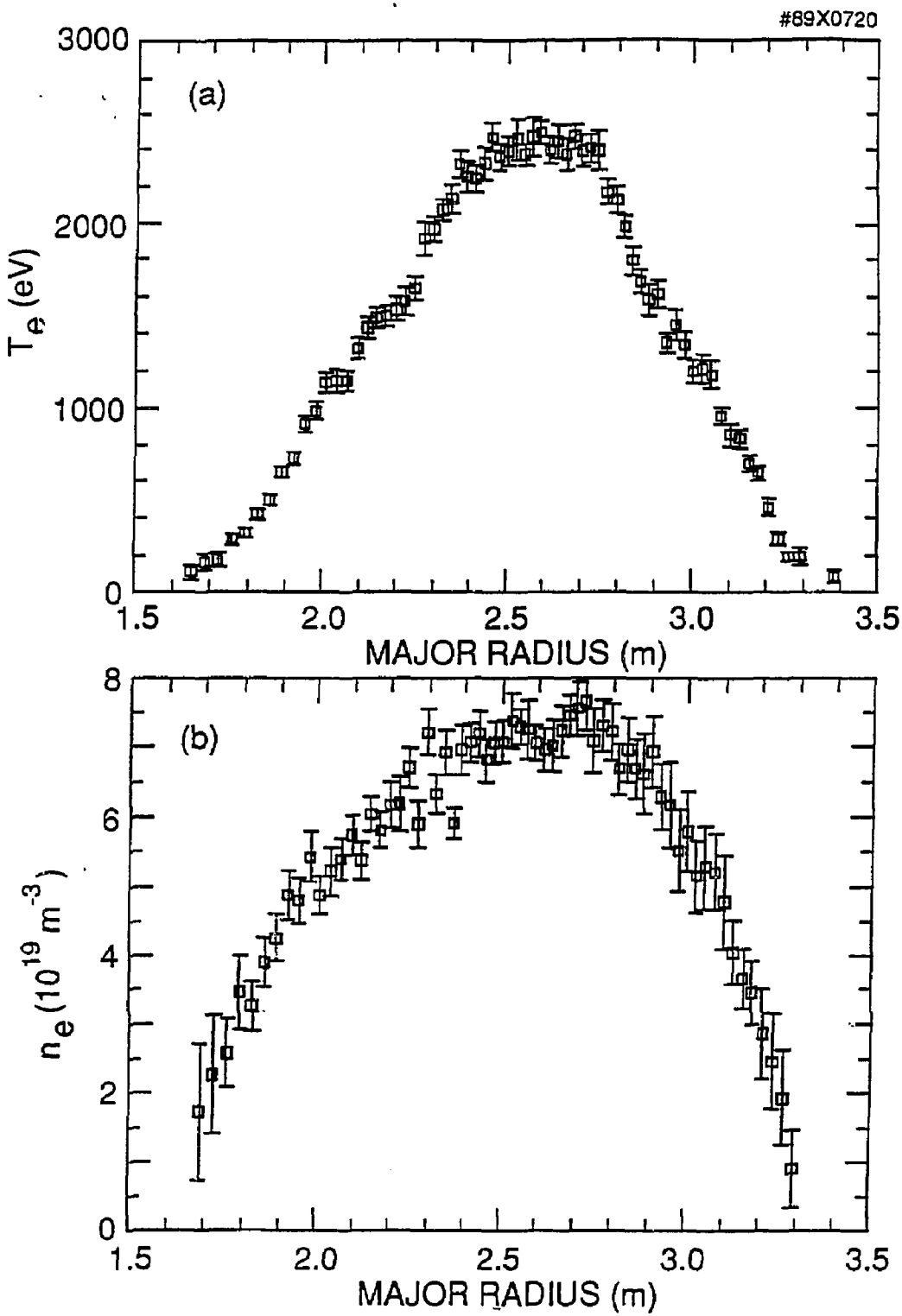
#89X0720
(a)
3000
2000
1000
0
T_e (eV)
1.5
2.0
2.5
3.0
3.5
MAJOR RADIUS (m)
(b)
8
6
4
2
0
$n_e (10^{19}\ m^{-3})$
1.5
2.0
2.5
3.0
3.5
MAJOR RADIUS (m)

FIG. 2

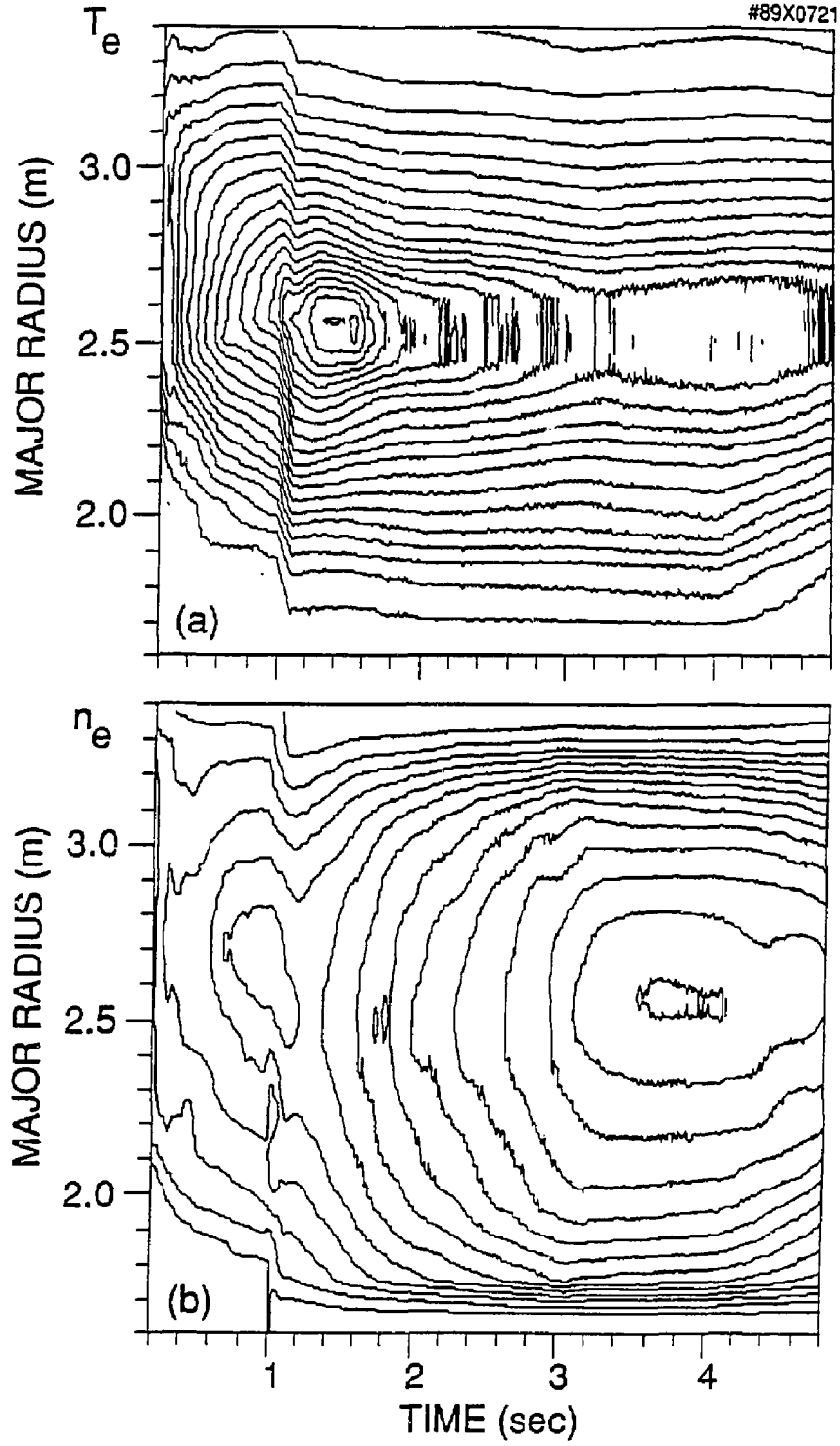
#89X0721
T_e
3.0
2.5
2.0
MAJOR RADIUS (m)
(a)
n_e
3.0
2.5
2.0
MAJOR RADIUS (m)
(b)
1
2
3
4
TIME (sec)

FIG. 3

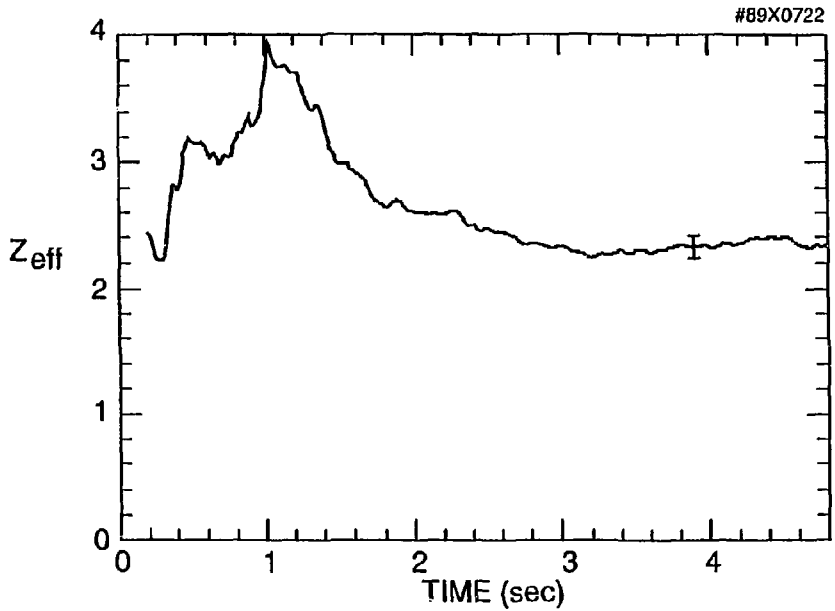

FIG. 4

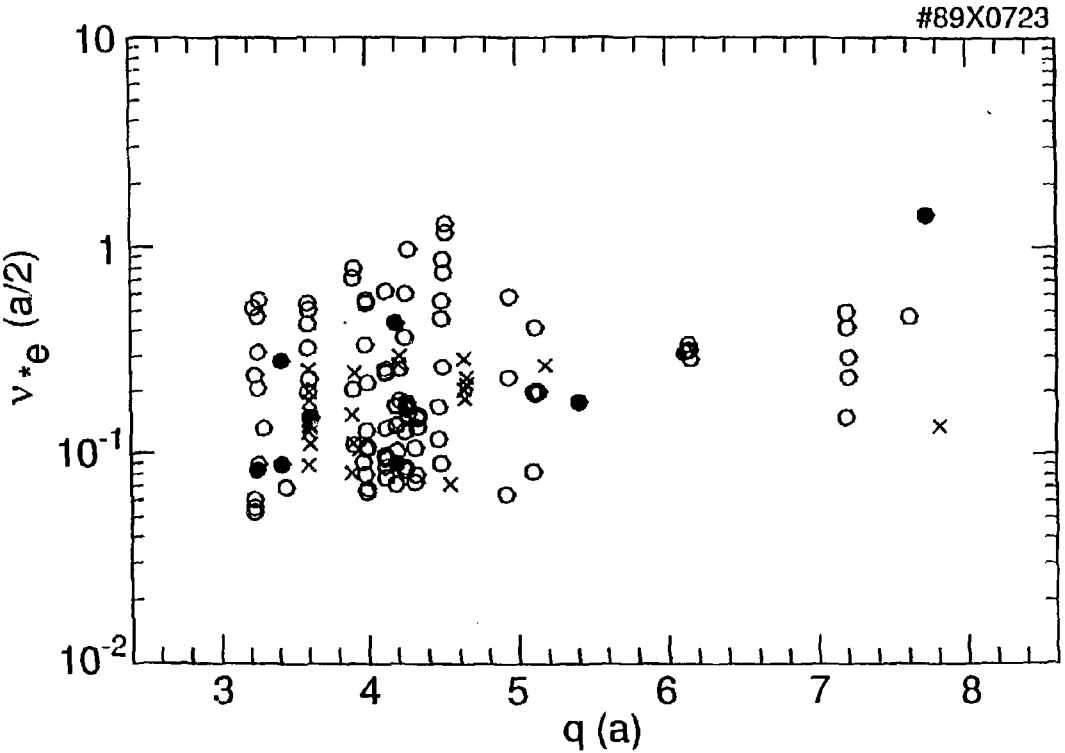

FIG. 5

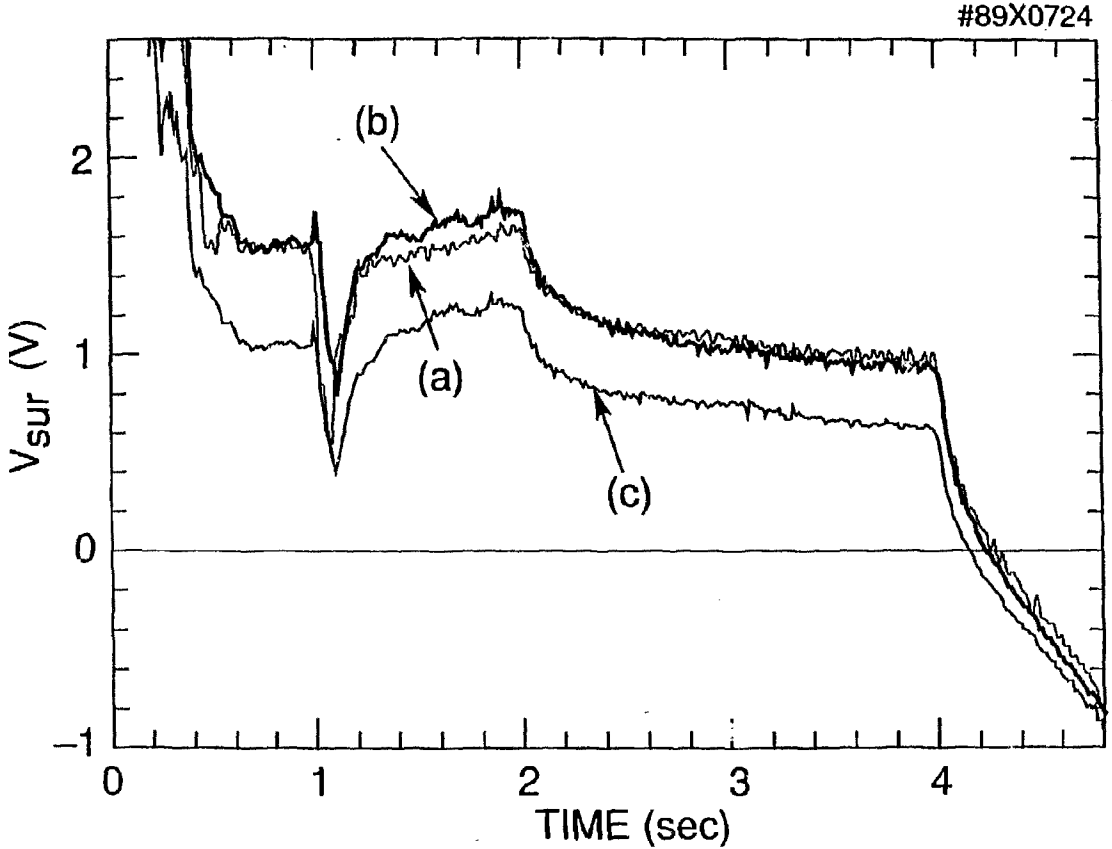

FIG. 6

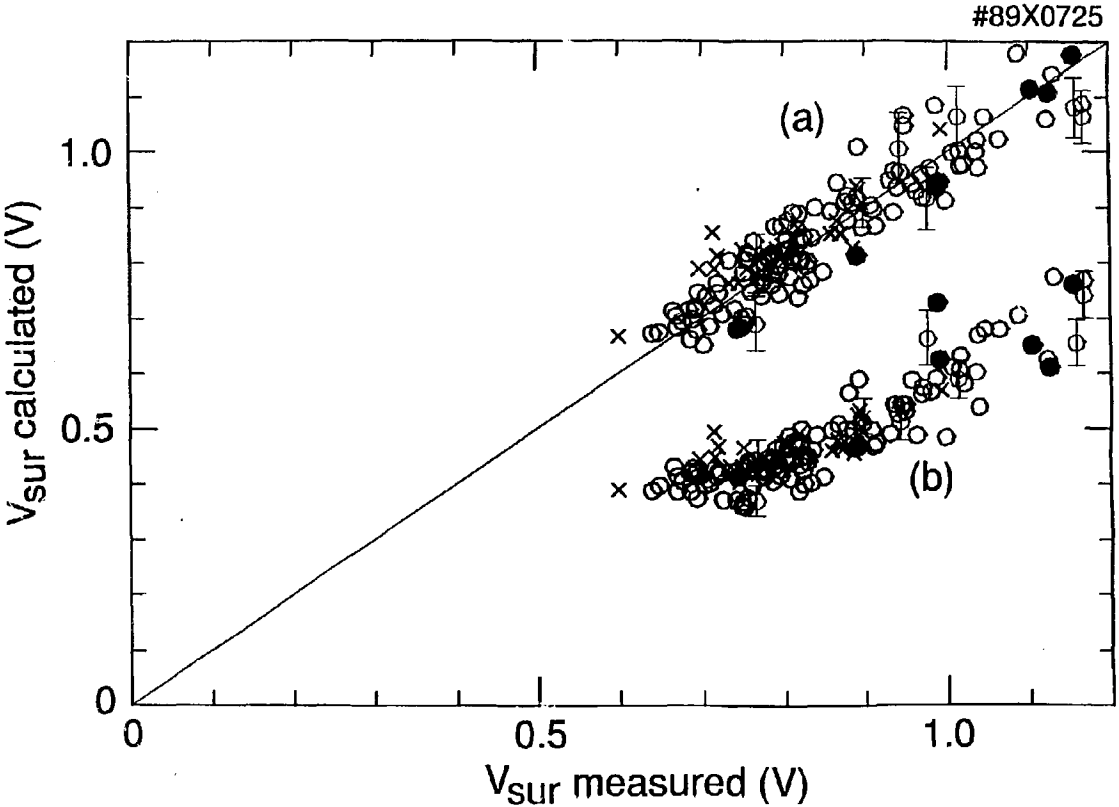

FIG. 7

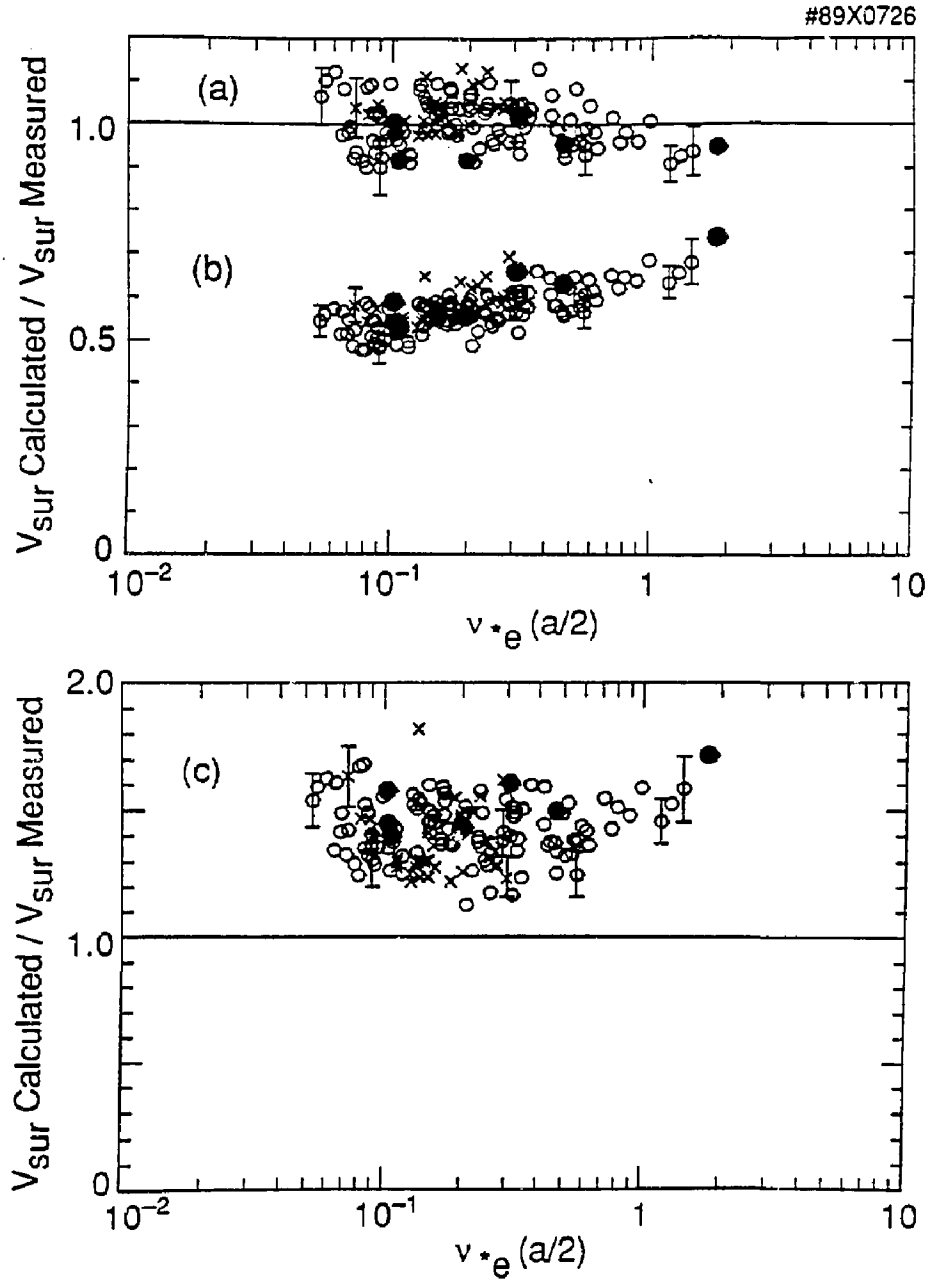
#89X0726
(a)
(b)
(c)
1.0
0.5
0
2.0
V_{sur} Calculated / V_{sur} Measured
10^{-2}
10^{-1}
1
10
ν_{*e} (a/2)

FIG. 8

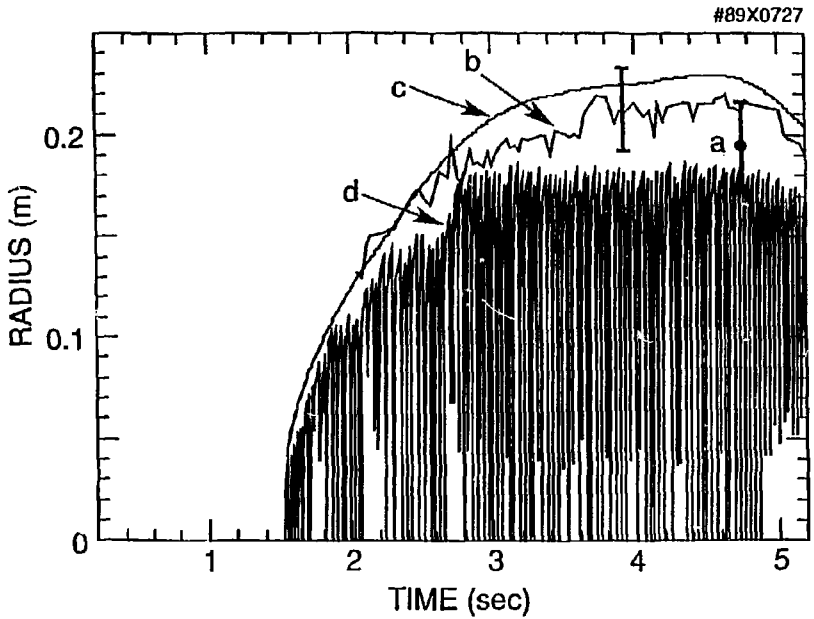

FIG. 9